DOI: 10.1002/chem.201000111

Mechanisms of Singlet-Oxygen and Superoxide-Ion Generation by Porphyrins and Bacteriochlorins and their Implications in Photodynamic Therapy

Elsa F. F. Silva,[a] Carlos Serpa,[a] Janusz M. Dąbrowski,[b] Carlos J. P. Monteiro,[a] Sebastião J. Formosinho,[a] Grazyna Stochel,[b] Krystyna Urbanska,[c] Sérgio Simões,[d] Mariette M. Pereira,[a] and Luis G. Arnaut*[a]

Abstract: New halogenated and sulfonated bacteriochlorins and their analogous porphyrins are employed as photosensitizers of singlet oxygen and the superoxide ion. The mechanisms of energy and electron transfer are clarified and the rates are measured. The intermediacy of a charge-transfer (CT) complex is proved for bacteriochlorins, but excluded for porphyrins. The energies of the intermediates and the rates of their interconversions are measured, and are used to obtain the efficiencies of all the processes. The mechanism of formation of the hydroxyl radical in the presence of bacteriochlorins is proposed to involve a photocatalytic step. The usefulness of these photosensitizers in the photodynamic therapy (PDT) of cancer is assessed, and the following recommendations are given for the design of more effective PDT protocols employing such photosensitizers: 1) light doses should be given over a more extended period of time when the photosensitizers form CT complexes with molecular oxygen, and 2) Fe^{2+} may improve the efficiency of such photosensitizers if co-located in the same cell organelle assisting with an in vivo Fenton reaction.

Keywords: charge transfer · photodynamic therapy · photosensitizers · porphyrinoids · radical ions · singlet oxygen

Introduction

Porphyrins, phthalocyanines, and related macrocycles have substantial electronic absorptions in the "phototherapeutic window" (650–900 nm, in which tissues are most transparent), high singlet-oxygen-producing ability, and some tendency to accumulate in solid tumours. These properties have made them the most studied class of molecules for application as photosensitizers in the photodynamic therapy (PDT) of cancer. The design and synthesis of molecules exhibiting increased infrared absorptions and higher singlet-oxygen quantum yields (Φ_Δ) is a very active field of research,[1–5] and shows promise for becoming a key treatment method in oncology.[6–8] Further progress in this field will benefit from a better understanding of the interaction between the photosensitizer, light, and oxygen. This work addresses quantitatively that interaction when the photosensitizer is a porphyrin or a bacteriochlorin.

Photofrin® (a mixture of purified fractions of hematoporphyrin derivatives) and Foscan® (a synthetic chlorin) are the most widely used PDT photosenstitizers. More recently, bacteriochlorins have been enrolled in clinical trials of photodynamic therapy for various types of cancers,[9,10] because of their enhanced absorptions in the phototherapeutic window. Some reports have suggested that the efficacy of bacteriochlorins in PDT is due not only to their strong infrared absorbance and their ability to transfer a large part of their

[a] E. F. F. Silva, Dr. C. Serpa, C. J. P. Monteiro, Prof. S. J. Formosinho, Prof. M. M. Pereira, Prof. L. G. Arnaut
Chemistry Department, University of Coimbra
3004-535 Coimbra (Portugal)
Fax: (+351) 239-827-703
E-mail: lgarnaut@ci.uc.pt

[b] Dr. J. M. Dąbrowski, Prof. G. Stochel
Faculty of Chemistry, Jagiellonian University
Ingardena 3, 30-060 Kraków (Poland)

[c] Prof. K. Urbanska
Faculty of Biochemistry, Biophysics and Biotechnology
Jagiellonian University
Gronostajowa 7, 30-349 Kraków (Poland)

[d] Prof. S. Simões
Faculty of Pharmacy, University of Coimbra
3000 Coimbra (Portugal)

Supporting information for this article is available on the WWW under http://dx.doi.org/10.1002/chem.201000111.

triplet-state energy to molecular oxygen, with the consequent production of singlet oxygen ($^1\Delta_g$ O_2), but also to their ability to transfer an electron to molecular oxygen and generate the superoxide ion ($O_2^{\bullet-}$).[11–13] It has been noted that tumour cells have diminished amounts of the superoxide dismutase, and that superoxide radical production may be involved in PDT apoptosis.[14] This low level of superoxide dismutase in tumour cells suggests that photosensitizers capable of producing superoxide may be particularly effective in killing such cells. In view of the roles played by singlet oxygen and the superoxide ion in the oxidative stress and death of cells, it is particularly important to establish the mechanisms of energy transfer and electron transfer from the photosensitizers to molecular oxygen.

The ubiquity of molecular oxygen and its low-energy singlet excited state ($E_\Delta = 22.5\,\mathrm{kcal\,mol^{-1}}$), have made energy transfer from a photosensitizer to molecular oxygen one of the most prevalent and intensively investigated photochemical processes. The mechanism of this energy transfer is now close to reaching a consensus,[15] but disparate mechanisms have been proposed for the concomitant generation of superoxide. The current understanding of triplet-state quenching by molecular oxygen is based on the mechanism proposed by Wilkinson, Scheme 1.[16–18] This mechanism shows that the diffusion-controlled encounter of the excited triplet sensitizer and the triplet ground-state O_2 leads to the reversible formation of excited encounter complexes of singlet, triplet, and quintet multiplicities. Statistically, there will be one singlet, three triplets, and five quintet complexes. The quintet pathway has no spin- or energy-allowed products, and quenching occurs only through internal conversion processes in the singlet and triplet pathways. In the absence of charge-transfer interactions, the nCT channel, the triplet pathway is unproductive, the rate of formation of singlet oxygen is given by Equation (1), and the quantum yield of singlet-oxygen generation may reach $\Phi_\Delta = 1$.

$$\mathrm{k}_\Delta = \frac{\mathrm{k}_{\mathrm{diff}}\,{}^1k_\Delta}{9(k_{-\mathrm{diff}} + {}^1k_\Delta)} \leq \frac{k_{\mathrm{diff}}}{9} \qquad (1)$$

In the presence of charge transfer, the CT channel, and for small energetic differences between the singlet and triplet states of the intermediates, the rate-determining step is the parallel formation of singlet and triplet exciplexes; the limiting rate increases to $k_\Delta \leq {}^4/_9 k_{\mathrm{diff}}$, and the limiting quantum yield decreases to $\Phi_\Delta = 0.25$. Schmidt proposed a modification to this mechanism, based on detailed data on energy-transfer rates to higher electronic states of molecular oxygen, for which the intersystem crossing equilibrium is fully established between singlet and triplet pathways at the encounter complexes rather than at the charge-transfer complexes.[19,20]

This work presents a consistent mechanistic interpretation of singlet oxygen and superoxide generation from the triplet states of the porphyrins and bacteriochlorins illustrated here, based on kinetic modelling of spectroscopic, photoacoustic, and chemical data. Energy and electron transfers are exquisitely entangled in such systems, which are a fascinating playground for energy and electron-transfer models. We show that the quenching of porphyrin or bacteriochlorin triplet states by oxygen follows different reaction mechanisms. The bacteriochlorin triplet quenching involves charge-transfer species, and the quantum yield of reactive oxygen species (ROS: singlet oxygen, superoxide ion, hydrogen peroxide, hydroxyl radical) is increased when a given light dose is delivered at lower laser intensities over a more extended period of time. Additionally, the mechanism of hydroxyl radical formation suggests that the presence of ferrous ions may increase the yield of this ROS through the Fenton reaction. On the other hand, the quenching of porphyrin triplets by molecular oxygen leads essentially to singlet oxygen, and the quantum yield of its generation is less sensitive to laser intensities or adjuvants. The conclusion of this mechanistic study is that PDT with bacteriochlorins

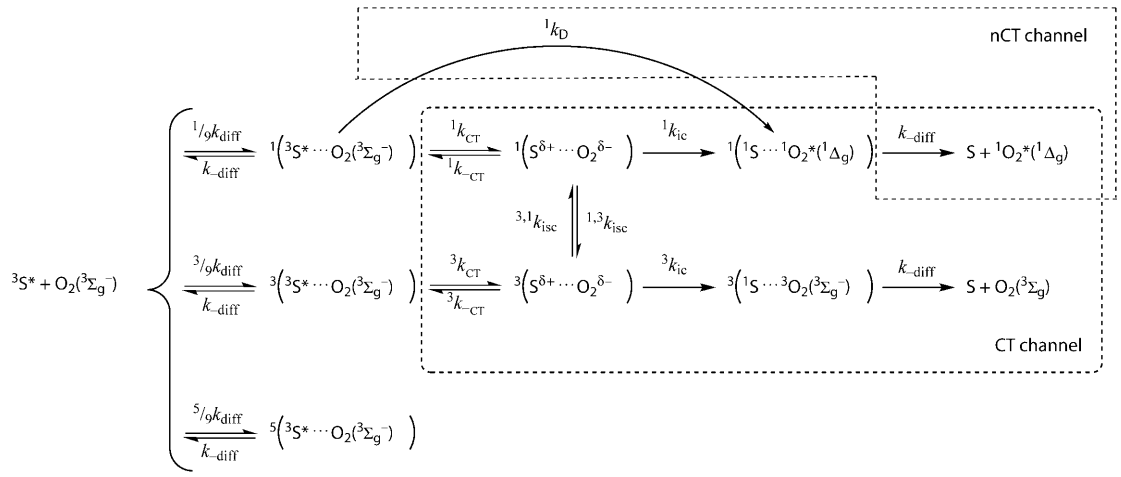

Scheme 1. Wilkinson mechanism for singlet-oxygen generation from the triplet state of a sensitizer, simplified under the assumption that intersystem crossing between encounter complexes is not efficient.

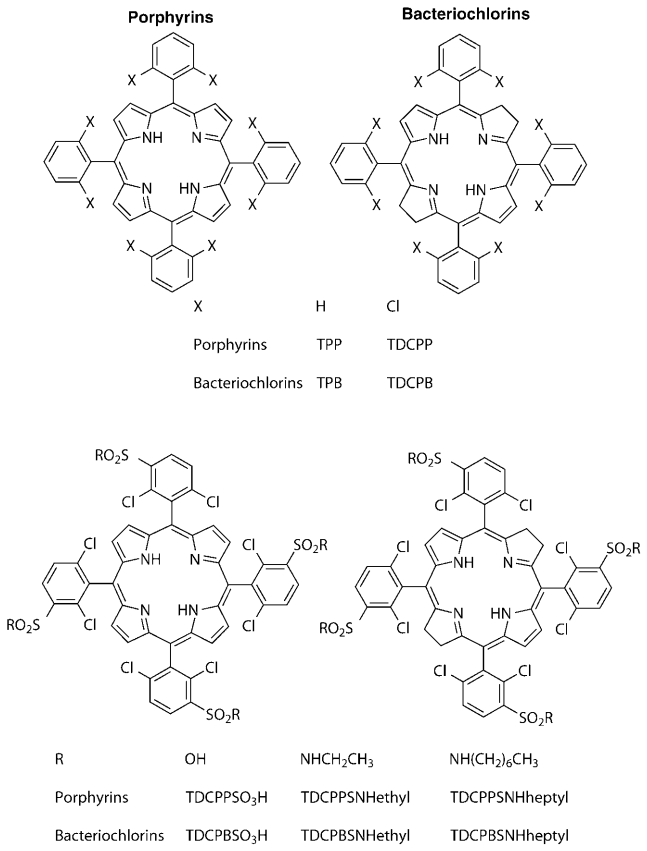

should be more effective at lower laser intensities, and in the presence of ferrous ions.

Results

Porphyrins and bacteriochlorins are very useful for addressing the mechanism of triplet-state quenching by molecular oxygen, because their triplet-state energies (E_T = 33 kcal mol^{-1} for tetraphenylporphyrin, TPP,[21] and 25–30 kcal mol^{-1} for analogous bacteriochlorins[4]) are lower than the energy of the second excited state of molecular oxygen ($^1\Sigma_g^+ O_2$, E_Σ = 37.5 kcal mol^{-1}). Hence, energy transfer to higher electronic states of molecular oxygen is not relevant to our systems, in contrast to the case for higher energy photosensitizers.[22] Additionally, the tetraphenylporphyrins and bacteriochlorins employed in this work have chlorine atoms in the *ortho*-positions of the phenyl rings, which reduce their singlet-state lifetimes to less than 1 ns, and make energy transfer from the singlet state of the sensitizers uncompetitive with intersystem crossing to the triplet state. This simplifies the mechanistic studies appreciably, because only one electronically excited state of the photosensitizer and one electronically excited state of molecular oxygen have to be taken into account.

Figure 1 shows the absorption and fluorescence spectra of TDCPPSNHethyl and TDCPBSNHethyl in ethanol, which are representative of our porphyrins and bacteriochlorins.

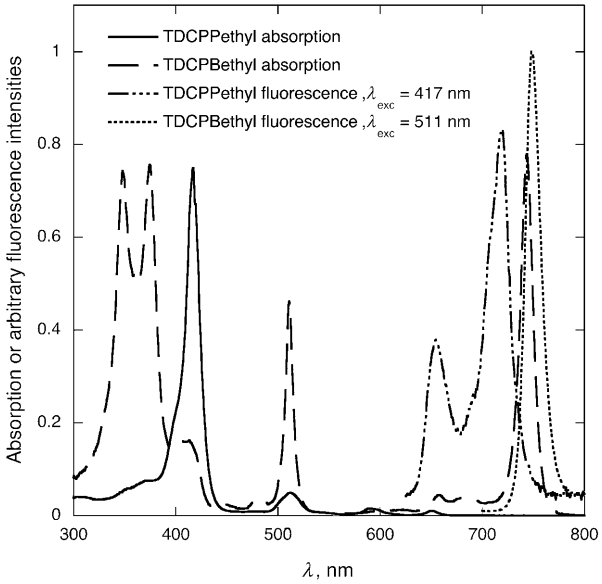

Figure 1. Absorption and fluorescence spectra of TDCPPSNHethyl and TDCPBSNHethyl in ethanol.

The intense absorption of the bacteriochlorin at λ_{max} = 745.5 nm is particularly remarkable. The absorption coefficient in the infrared, ε_{max} = 97000 M^{-1}cm^{-1}, is among the largest for non-aggregating molecules in polar solvents. The shoulder at 410 nm and the small peak at 658 nm are evidence of a small chlorin contamination, which is present in less than 5% in our samples. The chlorin red absorption band is 6–7 nm further displaced into the red than that of the corresponding porphyrin, which is typical of these molecules and allows for their assignment. With appropriate selection of excitation and emission wavelengths, this contamination does not affect our results.

Absorption and steady-state fluorescence data are collected in Table 1, together with literature data on related molecules. Both porphyrins and bacteriochlorins have small Stokes shifts between absorption and fluorescence emission, and the fluorescence quantum yields of 5,10,15,20-tetrakis(2,6-dichlorophenyl) porphyrins and bacteriochlorins are rather low, $\Phi_F < 0.02$. The reduced fluorescence is due to the

Table 1. Absorption and fluorescence data of sulfonyl and sulfamoyl porphyrins and bacteriochlorins in ethanol, and of related compounds in toluene.

	λ_{max} [nm]	ε_{max} [M^{-1}cm^{-1}]	λ_{em} [nm]	E_S [kcal mol^{-1}]	Φ_F
TPP[a]	649.8	9600	652/719	44.0	0.10
TDCPP[b]	660	2000	661/719	43.3	0.005
TDCPPSO$_3$H			654/720	43.8	–
TDCPPSNHethyl	652	5000	655/720	43.8	0.0167
TDCPPSNHheptyl			658/724	43.6	0.0172
TDCPB[c]	747.0	126000	748	38.3	0.012
TDCPBSO$_3$H	744.5	61000	748	38.3	0.0062
TDCPBSNHethyl	745.5	97000	749	38.3	0.0081
TDCPBSNHheptyl	746	76000	751	38.2	0.0082

[a] Reference [21]. [b] References [24] and [26]. [c] Reference [4].

internal heavy-atom effect produced by the chlorine atoms in the *ortho*-positions of the phenyl rings. As discussed elsewhere, such chlorine atoms provide enough spin-orbit coupling to enhance the intersystem crossing to the triplet state.[23,24] The singlet-state energy was obtained from the intersection of normalized absorption and emission bands. The 1-octanol/water partition coefficients, K_{OW}, of these photosensitizers range from log $K_{OW}=-1.80$ for $TDCPPSO_3H$ to log $K_{OW}>4$ for TDCPPSNHheptyl,[25] which emphasizes the wide range of water solubilities of the photosensitizers selected for this study.

The presence of chlorine atoms in the *ortho*-positions of the phenyl rings severely restricts the rotation of the single bond at the *meso*-position on 5,10,15,20-tetrakisphenyl porphyrins or bacteriochlorins. When the phenyl rings are unsymmetrical, geometric isomers result from the different position of the *ortho* and/or *meta* substituents relative to the porphyrin plane. Such atropisomers have been isolated for a series of 5,10,15,20-tetrakis(2,6-dichloro-3-sulfamoylphenyl) porphyrins, and shown to have substantially different spectroscopic properties.[27] Atropisomers are also present in the unsymmetrical molecules of Table 1, and the values reported here correspond to a weighted average of the properties of the individual atropisomers in the fractions collected after chromatography. However, this will not affect the rates and mechanisms discussed further below in this work.

Under our experimental conditions, no phosphorescence emission could be detected unambiguously from our molecules, as is generally the case for free-base porphyrins and related macrocycles.[28] Reports of phosphorescence from free-base bacteriochlorins must be regarded with caution,[29] as we also have been misled by the phosphorescence of impurities in free-base chlorin samples.[21,30] An alternative approach to measuring the triplet-state energies of these molecules is to use photoacoustic calorimetry (PAC).[21] This technique measures the heat deposited in the medium as the excited molecule decays by radiationless processes. The energy balance of Scheme 2 in de-aerated solutions gives, for the prompt release of heat, Equation (2), in which ϕ_1 is the fraction of energy release as prompt heat (less than 8 ns under our experimental conditions, associated lifetime $\tau_1<$ 8 ns), and $E_{h\nu}$ is the laser energy at the excitation wavelength ($E_{355}=80.5$ kcal mol^{-1}).

$$E_T\Phi_T = (1-\phi_1)E_{h\nu}-\Phi_F E_S \quad (2)$$

The values for the triplet quantum yields of 5,10,15,20-tetrakis(2,6-dichlorophenyl) porphyrins, chlorins, and bacteriochlorins are, to a good approximation, equal to $1-\Phi_F$, because of the internal heavy-atom effect.[4,21,30] The triplet energies of the halogenated molecules presented in Table 2 were calculated using $\Phi_T=1-\Phi_F$ and Equation (2).

Table 2. Triplet-state properties of sulfonyl and sulfamoyl porphyrins and bacteriochlorins in ethanol, and of related compounds in toluene.

	E_T [kcal mol^{-1}]	τ_T (N_2) [μs]	τ_T (air) [ns]	k_q [M^{-1}s^{-1}]
TPP[a]	33.0[b]	43	349	1.4×10^9
TDCPP[c]		17	641	8.6×10^8
$TDCPPSO_3H$		40	855	5.4×10^8
TDCPPSNHethyl	33.0	38	710	6.6×10^8
TDCPPSNHheptyl	36.1	41	758	6.2×10^8
TDCPB[c]	30.4	32	257	2.1×10^9
$TDCPBSO_3H$		33	226	2.1×10^9
TDCPBSNHethyl	25.7	38	265	1.8×10^9
TDCPBSNHheptyl	27.4	28	295	1.6×10^9

[a] Reference [26]. [b] Reference [31]. [c] Reference [4].

Triplet-state lifetimes in aerated and N_2-saturated solutions were measured by laser flash photolysis, and Figure 2 shows representative decays. We were unable to detect the presence of long-lived intermediates other than triplets. Additionally, isosbestic points were observed for the ground-state recovery and triplet decay, indicating that at least 90%

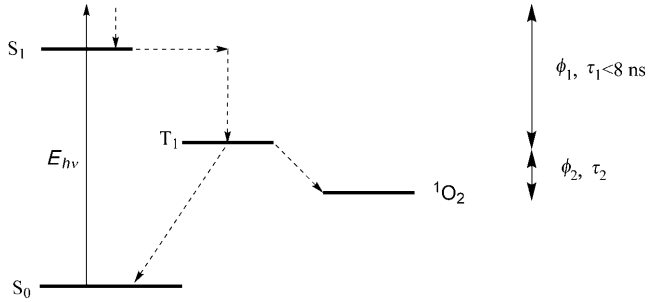

Scheme 2. Fractions of heat released (ϕ_1, ϕ_2) measured by PAC following pulsed laser irradiation of a sensitizer, S. In the presence of oxygen, the decay of the triplet state is also observed.

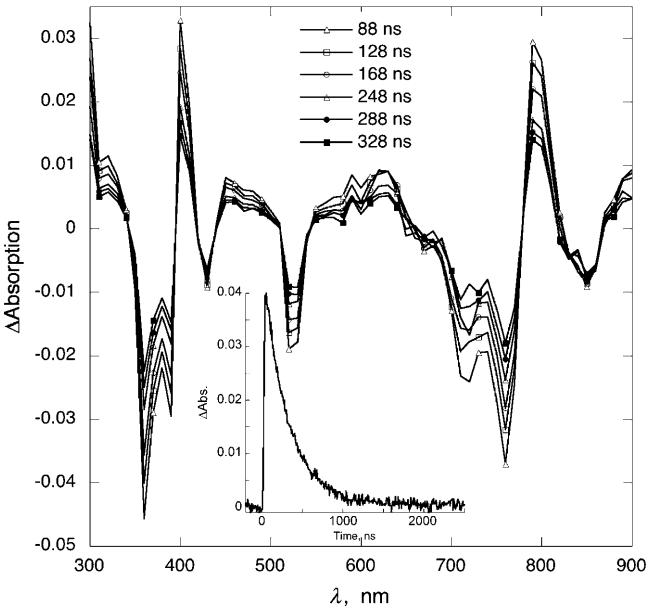

Figure 2. Transient absorption spectrum of TDCPBSNHheptyl in ethanol, measured by laser flash photolysis. The inset shows the decay at 400 nm, which has the same lifetime as the ground-state bleaching recovery.

of the triplet state returns to the ground state without kinetically relevant intermediates. The presence of oxygen substantially reduces the lifetimes of the triplet states, as shown in Table 2. The quenching rate constant was estimated from Equation (3), using the oxygen concentration in the appropriate solvent ($[O_2]=2.1\times10^{-3}$ M and 1.8×10^{-3} M in ethanol and toluene at 20 °C, respectively).[32] The data in Table 2 were collected at room temperature (approximately 20 °C).

$$1/\tau(\text{air}) = 1/\tau(N_2) + k_q[O_2] \quad (3)$$

Singlet oxygen in ethanol or toluene has a relatively long lifetime: 15.2[33] and 33 μs,[4] respectively. This favours the detection of the singlet-oxygen emission at 1270 nm. The singlet-oxygen lifetimes measured in this work are in very good agreement with the literature, as seen in Table 3.

Table 3. Singlet-oxygen rise time, decay, and quantum yield generated by sulfonyl and sulfamoyl porphyrins and bacteriochlorins in ethanol, or by related compounds in toluene.

	$\tau_{risetime}$ [ns]	τ_{decay} [μs]	Φ_Δ	k_1/k_n [M^{-1}]	$\Phi_{CT}E_{CT}$[a]
phenalenone			0.95[b]	0.02±0.01	
TPP		31.2[c]	0.71[c]		
TDCPP			0.98[d]		
$TDCPPSO_3H$	810	14.6	1.00	0.10±0.05	
TDCPPSNHethyl	743	14.7	0.85	0.10±0.05	≈0
TDCPPSNHheptyl	844	14.5	0.85	0.10±0.05	≈0
TDCPB[e]		33	0.60		10.4
$TDCPBSO_3H$	223	15.4	0.85	1.0±0.2	
TDCPBSNHethyl		13.7	0.66	1.0±0.2	8.1
TDCPBSNHheptyl	330	14.3	0.63	1.0±0.2	10.1

[a] Maximum error of ±2 kcal mol^{-1}. [b] In reference [34]. [c] In reference [4], 0.78±0.04 was reported from a third degree polynomial fit to the singlet-oxygen decay in benzene in reference [35], and 0.67±0.14 was reported from PAC studies in toluene in reference [21]. [d] From PAC studies in toluene in reference [26]. [e] From reference [4] in toluene.

The intensity of the singlet-oxygen phosphorescence decay extrapolated to time zero (I_Δ^0) can be used to determine the quantum yield of singlet-oxygen generation (Φ_Δ) by our photosensitizers using phenalenone as a reference.[36] The standard procedure employs values of I_Δ^0 measured at different laser intensities for solutions of samples and the reference with the same absorbance at the excitation wavelength. Special care must be exercised with systems that exhibit different degrees of non-linearity with the laser intensity.[35,37] The correct interpretation of the laser energy dependence of the singlet-oxygen emission intensity plots relies on the solution of the kinetic equations of Wilkinson's mechanism. A solution that retains the essential features of this mechanism is discussed further below, and it is shown that it supports the use of a linear fit to I_Δ^0, using the lowest laser energy measurements to obtain Φ_Δ. The data obtained with this procedure are presented in Table 3, and the linear fits can be found in the Supporting Information.

In direct energy transfer from the photosensitizer triplet state to molecular oxygen, the rise time of singlet-oxygen emission, $\tau_{risetime}$, must correspond to the decay rate of the triplet-state absorption in aerated solutions, τ_T(air). The fast rise time of the weak emission of singlet oxygen could only be observed using picosecond excitation of the bacteriochlorins (Figure 3). Nanosecond laser pulses produced too much interference with the singlet-oxygen rise time for such photosensitizers. A detailed kinetic analysis of the energy-transfer mechanism provides further insight into the observed rise times and decays, but Tables 2 and 3 show that $\tau_{risetime}$ and τ_T(air) have similar values for each system.

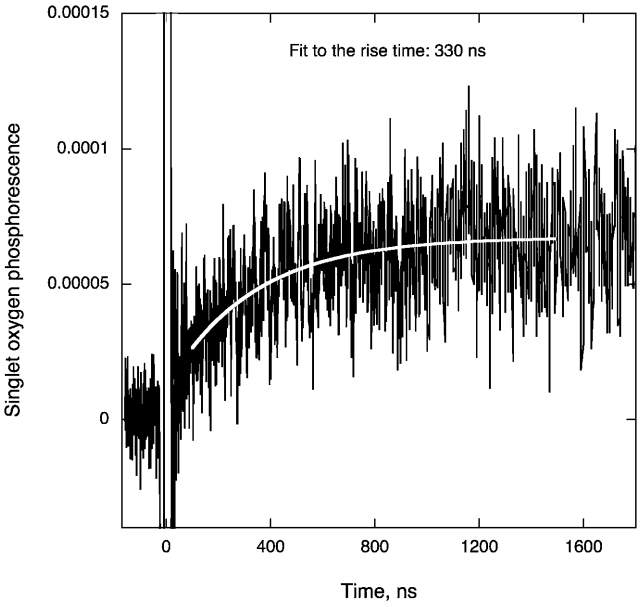

Figure 3. Rise time of singlet-oxygen emission following picosecond laser excitation of TDCPBSNHheptyl in ethanol.

Figure 4 presents EPR spectra in the presence of $TDCPBSO_3H$ measured in a phosphate buffer water solution (PBS, pH 7.4) with air-saturated solutions in the dark (Figure 4A), and an air-saturated solution irradiated for 12 min with the diode laser (Figure 4B). The computer simulation of this spectrum is shown for comparison in Figure 4C. The hydroxyl adducts spectrum was simulated on the basis of two conformers (see Figure 4D and E) undergoing chemical exchange. The line shape and the hyperfine (hf) splitting of the signal are typical of BMPO–OH radicals (BMPO = 5-tert-butoxycarbonyl 5-methyl-1-pyrroline *N*-oxide). The EPR parameters of BMPO adducts are presented in Table 4. Following earlier work,[38] we assign the spectrum in Figure 4B to a mixture of diastereomers of the BMPO–OH adduct.

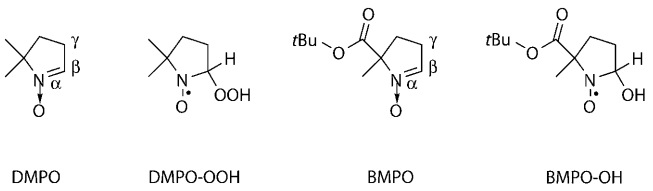

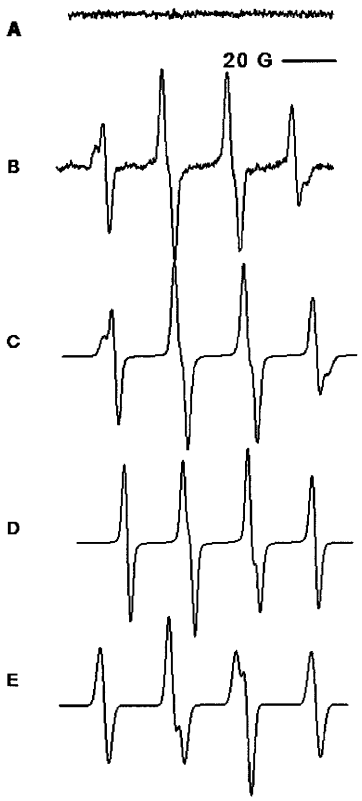

Figure 4. EPR spectrum of the BMPO−OH adduct observed during the illumination of $TDCPBSO_3H$ (50 μM) in PBS and in the presence of BMPO (40 mM): A) before illumination, B) during illumination of an air-saturated sample, C) simulation, D,E) simulation of two conformers of the BMPO−OH adduct.

Table 4. EPR parameters of BMPO−OH and DMPO−OOH adducts.

Spin adduct	Diastereomers [%]	Hyperfine coupling constant [G]		
		a_N	$a_{H\beta}$	$a_{H\gamma}$
[^{14}N]BMPO−OH	73	14.1	12.8	0.68
	27	14.2	15.8	0.77
[^{14}N]DMPO−OOH	–	13.3	10.6	1.34

Similar experiments were conducted with DMPO (5,5-dimethylpyrroline-*N*-oxide) in DMSO. We detected the $^{\bullet}$OOH adduct in the presence of air and light; the EPR spectrum of this adduct is presented in Figure 5B. However, in the absence of light, or in a nitrogen-saturated solution, or in the presence of superoxide dismutase, this adduct was not observed. Figure 5C shows the simulation of the DMPO−$^{\bullet}$OOH adduct. The line shape and the hyperfine (hf) splitting of the signal are typical of DMPO−OOH radicals generated by the reaction of DMPO and $O_2^{\bullet-}$ ($a_N = 13.3$ G, $a_{H\beta} = 10.6$ G, $a_{H\gamma} = 1.34$ G).

Singlet-oxygen and superoxide-ion generation in ethanol was further investigated with PAC. In aerated solutions, the decay of the triplet state occurs in the time window of the experiment, and is measured as a second fraction of heat decay, ϕ_2, with a lifetime τ_2 that corresponds to the triplet lifetime (Scheme 2). The heat decay in this time window has

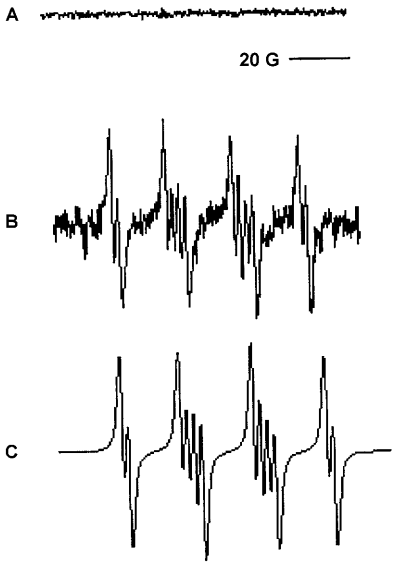

Figure 5. EPR spectrum of the DMPO−OOH adduct observed during the illumination of $TDCPBSO_3H$ (50 μM) in DMSO in the presence of DMPO (100 mM): A) before illumination, B) during illumination of an air-saturated sample, and C) simulation.

the contributions described by Equation (4), in which the singlet-oxygen energy is $E_\Delta = 22.5$ kcal mol^{-1}, $E_T\Phi_T$ is known from the prompt release of energy, [Eq. (2)], and is consistent with $\Phi_T \approx 1$ for all 5,10,15,20-tetrakis(2,6-dichlorophenyl) porphyrins and bacteriochlorins.

$$\phi_2 E_{h\nu} = \Phi_\Delta(E_T - E_\Delta) + \Phi_{CT}(E_T - E_{CT}) + (\Phi_T - \Phi_\Delta - \Phi_{CT})E_T \quad (4)$$

Figure 6 shows representative PAC waves measured in aerated ethanol solutions of the photosensitizers used in this study. The energy released in the formation of the charge-separated state, $\Phi_{CT}E_{CT}$, was calculated from Equation (4) with the value of Φ_Δ in Table 3.

Discussion

The discussion of the data is divided into three parts: a brief overview based on a simplified mechanism that retains the essential features of Wilkinson's mechanism, a detailed analysis of the mechanism of singlet-oxygen generation, and a mechanistic interpretation of the evidence for the formation of other reactive oxygen species ($O_2^{\bullet-}$, H_2O_2, and $OH^{\bullet}$).

The most immediate facts that emerge from this work are as follows. In de-oxygenated ethanol solution, halogenated tetraphenylporphyrins and bacteriochlorins have long-lived triplet states, formed with near unit quantum yields, but the quenching of such triplet states by molecular oxygen is distinctly different. Porphyrin triplets are quenched with a rate constant $k_q = 6 \times 10^8$ M^{-1}s^{-1}, which is virtually identical to $^1/_9 k_{diff}$, in which $k_{diff} = 5.4 \times 10^9$ M^{-1}s^{-1} in ethanol at 20 °C.[32]

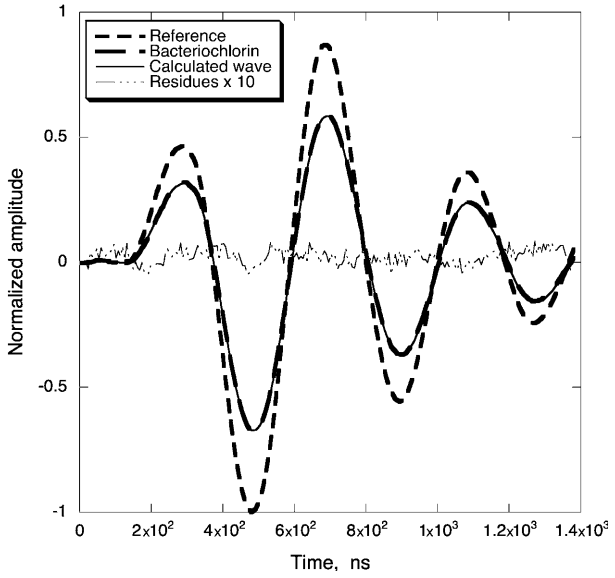

Figure 6. Photoacoustic calorimetry waves of reference (short dashed line) and TDCPBSNHethyl (long dashed line) in aerated ethanol solutions following 355 nm laser excitation. The calculated wave was obtained by reconvolution of the decay parameters with the reference wave, and its difference from the TDCPBSNHethyl wave, called the residue, was scaled by a factor of 10 to make it more visible in the plot.

On the other hand, bacteriochlorin triplets are quenched with a rate constant $k_q = 2\times10^9\,\mathrm{M^{-1}s^{-1}}$, which approaches $^4/_9 k_{diff}$. The singlet-oxygen phosphorescence quantum yields of such porphyrins and bacteriochlorins are also different: whereas porphyrin triplets generate singlet oxygen with an efficiency near unity, the corresponding value for bacteriochlorins is 40–15% lower. It must be emphasized that the triplet state of TPP also generates singlet oxygen with unit efficiency, because its triplet quantum yield in toluene is $\Phi_T = 0.73 \pm 0.10$.[21] According to Wilkinson's mechanism, porphyrins follow the nCT channel, but bacteriochlorins predominantly follow the CT channel. Additionally, our data show that both energy and electron transfers take place from the bacteriochlorin triplet states to molecular oxygen, leading to singlet oxygen and the superoxide ion, respectively.

The molecular understanding of the phenomena summarized above can be built on the simplified mechanism shown in Scheme 3, which retains the essential features of Wilkinson's mechanism, but is more amenable to an analytical solution. The approximations involved in the simplified mechanism and in its kinetic analysis are presented in detail in the Supporting Information. Two features of this mechanism must be emphasized: 1) the simplified mechanism explicitly considers the formation of the superoxide ion from the charge-separated complex, which may be energetically favourable in polar solvents; 2) the simplified mechanism does not consider the decay of $^1O_2$, and consequently $[^1O_2]_\infty$ is proportional to I_Δ^0, which is a measure of the total amount of singlet oxygen produced by the photosensitizer.

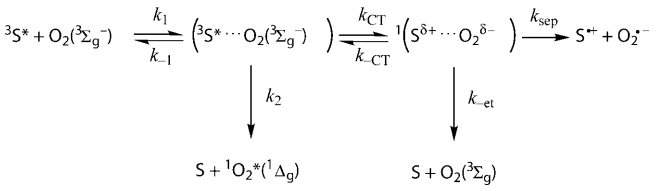

Scheme 3. Simplified mechanism of photosensitizer quenching, together with singlet-oxygen and superoxide-ion generation.

For low-to-moderate light intensities, using the steady-state approximation for $(^3S^*\cdots O_2{}^3\Sigma_g^-)$ and $(S^{\delta+}\cdots O_2^{\delta-})$ in the simplified mechanism, and subject to the condition that $[S^*] \ll [O_2]$, the concentration of singlet oxygen when $t\to\infty$ is given by Equation (5), in which $k_n = k_{-1} + k_2 + k_3 k_{CT}/(k_3 + k_{-CT})$, $k_{1CT} = k_1(1 + k_{CT}/(k_3 + k_{-CT}))$ and $k_3 = k_{sep} + k_{-et}$, and it is assumed that $[^3S^*\cdots O_2{}^3\Sigma_g^-] + [S^{\delta+}\cdots O_2^{\delta-}] \ll [O_2]$.

$$[^1O_2]_\infty = \frac{k_n}{k_{1CT}} \frac{k_2}{k_2 + k_3 k_{CT}/(k_3 + k_{-CT})} \ln\left(1 + \frac{k_{1CT}}{k_n}[S^*]_0\right) \quad (5)$$

Below, we will represent $[S^{\delta+}\cdots O_2^{\delta-}]$ by $[S^{\bullet+}\cdots O_2^{\bullet-}]$, because for the cases where charge transfer is most relevant, a full charge transfer takes place.

For the absorbances employed in this work, $[S^*]_0$ is nearly identical to the number of photons absorbed, $I_a = I_0(1-10^{-A})$, per unit volume. Thus, we expect the functional dependences of $[^1O_2]$ versus $[S^*]_0$ and I_Δ^0 versus $E_{h\nu}$ to be identical. Figure 7 presents fits of expressions with the form of Equation (5) to the values of I_Δ^0 measured for a wide range of laser energies $E_{h\nu}$. The fitting is remarkably good in view of the approximations involved and of the wide range of laser energies employed. It is important to emphasise that the singlet-oxygen quantum yields presented in Table 3 were not obtained from this fit, but from the linear fit to the lower laser energies. Such linear fits are shown in the Supporting Information.

The limit of Equation (5) for low laser energies (low $[S^*]_0$), is the expression in Equation (6), which supports the linear fit employed to obtain the value of Φ_Δ presented in Table 3.

$$[^1O_2]_\infty = \frac{k_2}{k_2 + k_3 k_{CT}/(k_3 + k_{-CT})}[S^*]_0 \quad (6)$$

In principle, it is possible to deduce Φ_Δ from the fits in Figure 7. In practice, the term k_1/k_n can only be precisely determined when the curvature of the phenalenone-sensitized $^1O_2$ emission is appreciable, and this only occurs for very high laser energies, for which the approximations involved in deriving Equation (5) are no longer valid. Figure 7 indicates the values of k_1/k_n that give acceptable fits to Equation (5). The procedure that we recommend to obtain Φ_Δ consists in using the linear portion of the I_Δ^0 versus $E_{h\nu}$ dependence, and, on the basis of Equation (6), calculating Φ_Δ from the ratio of the slopes of that dependence for a sample and a reference with known Φ_Δ.

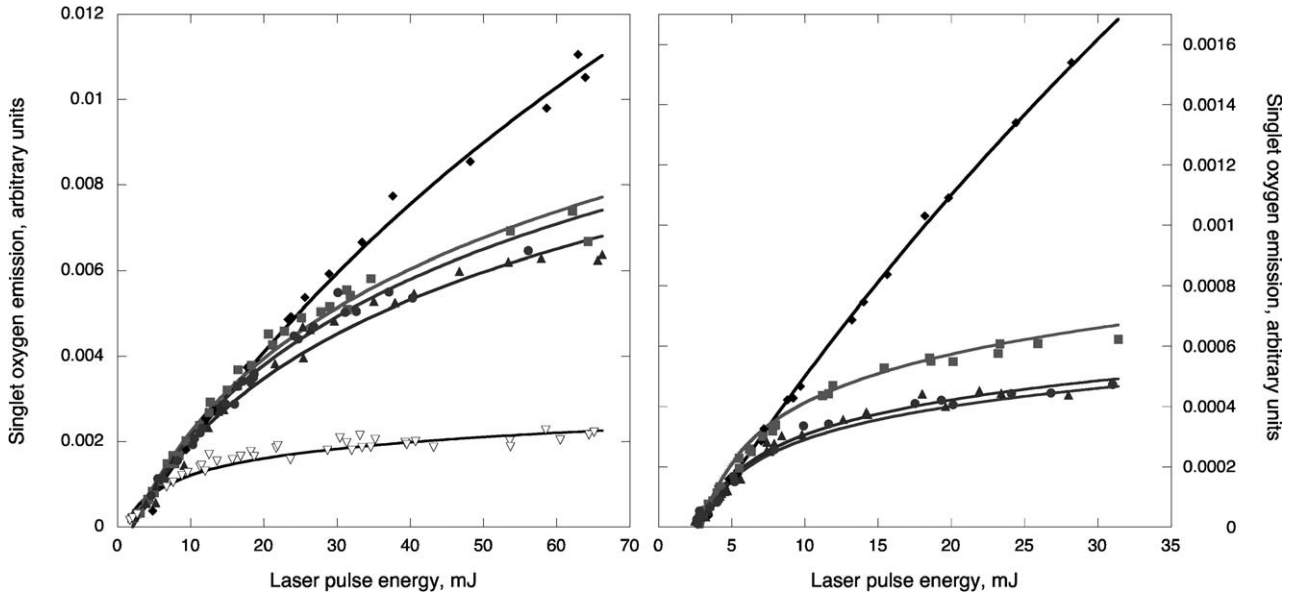

Figure 7. Extended laser energy dependence of singlet-oxygen emission in two independent experiments. ◆ = phenalenone. Left: ■ = TDCPPSO$_3$H, ▲ = TDCPPSNHethyl, ● = TDCPPSNHheptyl, △ = TDCPBSNHethyl. Right: ■ = TDCPBSO$_3$H, ▲ = TDCPBSNHethyl, ● = TDCPBSNHheptyl. The curves were fitted to an equation of the form of Equation (5) with $k_{1CT}/k_n = 0.02$, 0.1, or 1.0 for phenalenone, porphyrins, and bacteriochlorins, respectively. The pre-logarithmic factors in the left graph were 0.031, 0.0083 ± 0.0006, and 0.00124 for phenalenone, porphyrins, and bacteriochlorins, respectively

The resolution of the simplified mechanism kinetics also relates the observed triplet lifetimes with the various rate constants of that mechanism. The concentrations of the sensitizers under our experimental conditions are in the 10^{-5} M range, and $[S^*] \gg [O_2]$. The quenching of the photosensitizer in the simplified mechanism can be effectively approximated as a pseudo-first-order reaction, and the decay of the photosensitizer triplet state and the generation of singlet oxygen are given by Equation (7), in which $k_1' = k_1[O_2]$.

$$[S^*] = [S^*]_0 \exp\left[-k_1\left(1 - \frac{k_{-1}}{k_n}\right)t\right]$$

$$[^1O_2] = \frac{k_2}{k_2 + k_3 k_{CT}/(k_3 + k_{-CT})}[S^*]_0\left\{1 - \exp\left[-k_1'\left(1 - \frac{k_{-1}}{k_n}\right)t\right]\right\} \quad (7)$$

As expected, the triplet-state decay and the singlet oxygen rise time have the same lifetimes (Figures 2 and 3, and Tables 2 and 3).

Singlet-oxygen generation: In the following, we combine our kinetic and thermochemical data with the data available in the literature to determine the rate constants of all the elementary steps identified in the simplified mechanism of Scheme 3, as well as to estimate the energies and quantum yields of the species invoked by that mechanism.

The observation of $k_q = {}^1/_9 k_{diff}$ in the quenching of triplet porphyrins has another implication for the triplet pathway. If the triplet encounter complex $^3\{^3S^*\cdots O_2\,^3\Sigma_g^-\}$ had a nanosecond lifetime, like the singlet state of TPP and related non-halogenated porphyrins, the increased spin-orbit coupling introduced by the presence of Cl atoms would promote intersystem crossing to $^1\{^3S^*\cdots O_2\,^1\Delta_g\}$ and increase k_q. The fact that k_q of porphyrins does not increase with halogenation suggests that the triplet encounter complex has a short lifetime, $(k_{-1} + k_2) > 10^9\ s^{-1}$. On the other hand, fast intersystem crossing must occur within the charge-separated states $^{1,3}\{S^{\bullet+}\cdots O_2^{\bullet-}\}$, as suggested by Wilkinson's mechanism. The kinetic analysis of the simplified mechanism does not need to identify the multiplicity of these states, provided that we employ $k_1 = {}^1/_9 k_{diff}$ for the nCT channel and $k_1 = {}^4/_9 k_{diff}$ for the CT channel.

The CT channel is expected to become relevant when charge-transfer complexes become as stable as the corresponding encounter complexes. Ethanol is a polar solvent ($\varepsilon = 24.55$), and the CT complexes are best regarded as radical–ion pairs with energies given by Equation (8).[39]

$$\Delta G_{rip}^{\varepsilon} = (E_D^{ox} - E_A^{red})^{\varepsilon} - \frac{e_0^2}{\varepsilon r_{DA}} \quad (8)$$

The last term in Equation (8) is negligible in ethanol. The half-wave reduction potential for oxygen ($E_A^{red} = -0.78$ V vs. SCE in DMSO,[40] also found in other sources[18]) and the half-wave oxidation potential for tetraphenylbacteriochlorin, TPB ($E_D^{ox} = 0.40$ V vs. SCE in CH_2Cl_2),[41] give a radical–ion pair energy of 27 kcal mol^{-1}, similar to the E_T of bacteriochlorins. A different situation is obtained with the half-wave oxidation potential for TPP ($E_D^{ox} = 1.13$ V vs. SCE in DMF),[42] which gives $\Delta G_{rip}^{\varepsilon} = 44$ kcal mol^{-1}, much higher than the E_T of porphyrins. Although different solvents were employed in these measurements and a quantitative comparison is not possible, the 10 kcal mol^{-1} endothermicity expected for the formation of $\{TPP^{\bullet+}\cdots O_2^{\bullet-}\}$ from $\{^3TPP\cdots O_2\}$ is in

sharp contrast with the possible exothermicity of the formation of $\{TPB^{\bullet+}\cdots O_2^{\bullet-}\}$ from $\{^3TPB\cdots O_2\}$. These estimates lend further support to the nCT channel in the quenching of triplet porphyrins by molecular oxygen, and to the early interruption of the triplet pathway.

Energy transfer in the encounter complex formed in the singlet pathway has been interpreted as an internal conversion of $^1\{^3S^*\cdots O_2{}^3\Sigma_g^-\}$ into $^1\{S\cdots O_2{}^1\Delta_g\}$, following an early suggestion by Kearns and co-workers.[43] This requires the encounter complex decay rate constant to follow the energy-gap law, and become slower as the triplet energy of the sensitizer increases, $\Delta E = E_\Delta - E_T$. Considering that the nCT channel has $\Phi_\Delta \approx 1$ and k_{CT} can be neglected, then $k_n \approx k_{-1} + k_2$, and the observed decay constant, $k_1'(1-k_{-1}/k_n)$ in Equation (7), can be rearranged to $k_1'k_2/(k_{-1}+k_2)$. Using the usual assumption that in the formation of encounter complexes with molecular oxygen, $k_{-diff}/k_{diff} \approx 1$ M,[20] we expect that $k_{-1}/k_1 \approx 1$ M. The observed decay constant takes the form $k_1k_2/(k_1+k_2)[O_2]$, and the energy-gap law should be observed when $k_2 < 0.1k_{-1}$. Figure 8 compares the energy-transfer rates from the triplet states of our porphyrins with those from other sensitizers.[44] The rate constants for the porphyrin triplets have reached the maximum possible value of the nCT channel, $k_1 = {}^1/_9 k_{diff}$, meaning that the Franck–Condon factors have been optimized.

Charge-transfer-induced quenching of triplet states is clearly observed in the quenching of substituted naphthalene triplet states by molecular oxygen in acetonitrile (Figure 9).[18] The quenching of triplet bacteriochlorins also follows the inverse correlation between the rates and efficiencies of singlet-oxygen generation observed when quenching proceeds through the CT channel. However, the energetics of the CT states in the bacteriochlorin systems

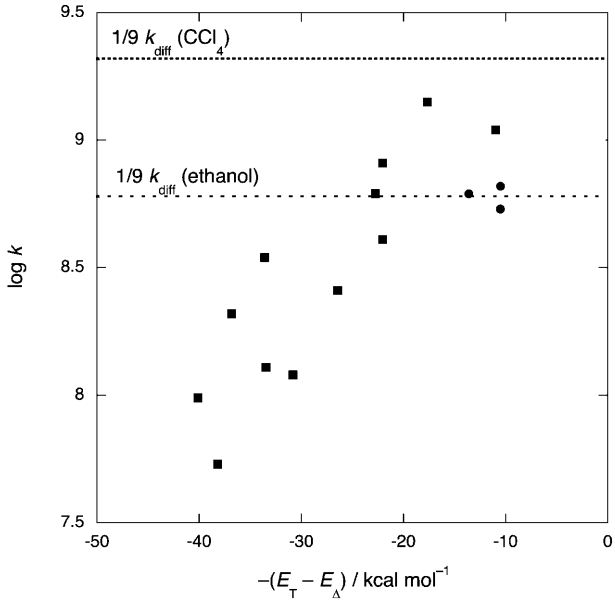

Figure 8. Energy gap law for triplets of TPP, ketones, quinones, and other aromatic molecules measured in CCl_4 (■), and for the porphyrins measured in this work in ethanol (●).

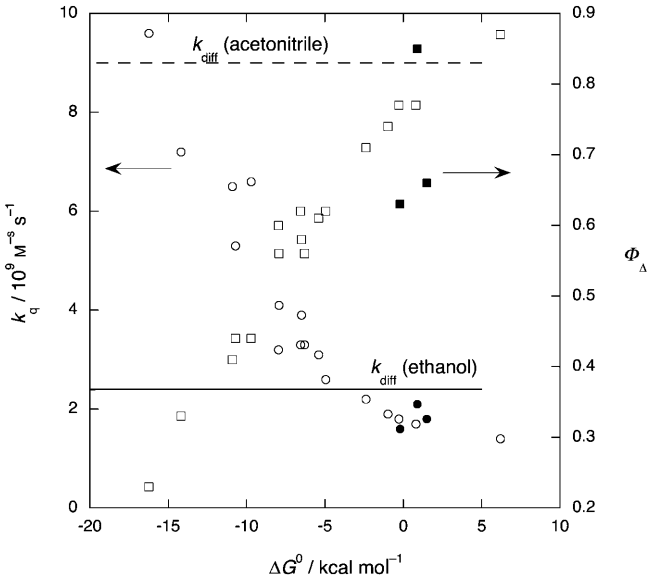

Figure 9. Rate constants (left axis, ●) and singlet-oxygen quantum yields (right axis, ■) for charge-transfer assisted quenching of substituted naphthalenes (open symbols) and bacteriochlorins (filled symbols).

are such that a noticeable acceleration is observed, but the efficiency of singlet-oxygen generation is not appreciably eroded. When k_{CT} is large, and consequently k_{-CT} is small, $k_n \approx k_{CT}$ and the triplet decay constant in Equation (7) approaches k_1'. Figure 9 shows that the limiting value is $k_1 = {}^4/_9 k_{diff}$, which can be assigned to efficient intersystem crossing between singlet and triplet charge-transfer complexes with sufficiently long lifetimes to reach equilibrium.

The semi-quantitative arguments presented above have quantitative expression in Equations (5)–(7). From the ratio k_{1CT}/k_n in Equation (5), and for the nCT channel (negligible k_{CT}), we obtain Equation (9).

$$\left(\frac{k_{1CT}}{k_n}\right)_{nCTchannel} = \frac{k_1}{k_{-1}+k_2} \tag{9}$$

With $k_1 = {}^1/_9 5.4\times10^9\,M^{-1}s^{-1}$, $k_{-1} = {}^1/_9 5.4\times10^9\,s^{-1}$, and the ratio fitted in Figure 7, $k_{1CT}/k_n \approx 0.1$ M for porphyrins, we obtain $k_2 = 5.4\times10^9\,s^{-1}$. This energy-transfer rate constant within the excited-state complex is also valid for the CT channel, because they differ only in the presence of a charge-transfer state of lower energy. In a finer analysis, it is arguable that k_2 refers to an internal conversion subject to the energy-gap law, and may be slightly higher for bacteriochlorins. However, porphyrin and bacteriochlorin triplet energies differ by only 5 kcal mol^{-1}, and it is reasonable to employ $k_2 = 5.4\times10^9\,s^{-1}$ also for our bacteriochlorins.

Another useful relation can be obtained by rearranging the time constant in Equation (7) to the form in Equation (10).

$$\frac{k_{-1}}{k_n} = 1 - \frac{1}{\tau_T k_1'} \tag{10}$$

From the ratio fitted in Figure 7 for bacteriochlorins which use the CT channel, we have $k_{1CT}/k_n \approx 1$ M, and k_n can be replaced by k_{1CT} in Equation (10). After some algebraic manipulation and using $k_{-1}/k_1 \approx 1$ M, we obtain Equations (11) and (12), in which τ_T is the triplet lifetime of the bacteriochlorin in the presence of oxygen.

$$k_3 = k_{-1} + (1 - k_1'\tau_T)k_2 \quad (11)$$

$$\frac{k_{CT}}{k_3 + k_{-CT}} = \frac{1}{k_1'\tau_T - 1} \quad (12)$$

With $k_1 = {}^4/_9 5.4\times10^9\ M^{-1}s^{-1}$, $[O_2] = 2.1\times10^{-3}$ M, $\tau_T = 260$ ns, and $k_2 = 5.4\times10^9\ s^{-1}$, we calculate $k_3 = 7.2\times10^8\ s^{-1}$. The value of k_3 and Equation (12) can be used to estimate the rate constants k_{CT} and k_{-CT}, because these are related by the free energy of formation of $\{S^{\bullet+}\cdots O_2^{\bullet-}\}$ from $\{^3S^*\cdots O_2\,^3\Sigma_g^-\}$, as shown in Equation (13), and this is given by the PAC data.

$$\frac{k_{CT}}{k_{-CT}} = \exp\left(-\frac{\Delta G^0_{CT}}{RT}\right) \quad (13)$$

Making $\Phi_{CT} = 0.33$ and 0.38 for TDCPBSNHethyl and TDCPBSNHheptyl, respectively, we obtain $E_{CT} = 24.7$ and 26.4 kcal mol^{-1}, which correspond to $\Delta G^0_{CT} = -1$ kcal mol^{-1} in both cases. This is consistent with Equation (8) and leads to $\Phi_\Delta + \Phi_{CT} = 1.00 \pm 0.01$. This value of ΔG^0_{CT}, together with Equation (12) and $k_3 = 7.2\times10^8\ s^{-1}$, give $k_{CT} = 5.7\times10^9\ s^{-1}$ and $k_{-CT} = 1.1\times10^9\ s^{-1}$. Table 5 lists the rates calculated for singlet-oxygen generation by porphyrins and bacteriochlorins.

Table 5. Typical rate constants in ethanol, $[O_2] = 2.1\times10^{-3}$ M, and other parameters relevant for kinetic modelling.

Rate constants	Porphyrins	Bacteriochlorins
k_{diff} [M^{-1}s^{-1}]	5.4×10^9	5.4×10^9
k_1 [M^{-1}s^{-1}]	$^1/_9\ k_{diff}$	$^4/_9\ k_{diff}$
$k_1' = k_1[O_2]$ [s^{-1}]	$^1/_9\ [O_2]\ k_{diff}$	$^4/_9\ [O_2]\ k_{diff}$
K_{-1} [s^{-1}]	k_1/1 M	k_1/1 M
$(k_{1CT}/k_n)_{exp}$ [M^{-1}]	0.10 ± 0.05	1.0 ± 0.2
k_2 [s^{-1}]	5.4×10^9	5.4×10^9
τ_T [ns]	800	260
k_3 [s^{-1}]		7.2×10^8
Φ_Δ	0.93 ± 0.08	0.7 ± 0.1
Φ_{CT}	0	0.3 ± 0.1
ΔG^0_{CT} [kcal mol^{-1}]	10	-1.0 ± 1
k_{CT} [s^{-1}]	negligible	5.7×10^9
k_{-CT} [s^{-1}]		1.1×10^9

An independent verification of the values in Table 5 is given by the product of the pre-logarithmic factor in Equation (4) by the factor multiplying $[S^*]_0$, which yields Equation (14).

$$\frac{k_2}{k_2 + k_3 k_{CT}/(k_3 + k_{-CT})} \quad (14)$$

The values fitted in Figure 7 give 8.5×10^{-4} for the porphyrins and 1.2×10^{-3} for the bacteriochlorins. Only the ratio between these values is meaningful because it cancels instrumental constants. Although the ratio given by the experimental data has a large uncertainty, 1.4 ± 0.76, it is reassuring that the same ratio calculated with the data in Table 4, 0.71, is within the experimental limits.

Superoxide-ion generation: The spectrum of the superoxide spin adduct of DMPO (DMPO–OOH) shown in Figure 5 is prima facie evidence for the formation of the superoxide ion in DMSO. However, the EPR spectra obtained after illumination of TDCPBSO$_3$H aqueous solutions in the presence of BMPO show the formation of a spin adduct between this spin trap and the hydroxyl radical (BMPO–OH). In this section we discuss the generation and decay of the superoxide ion, including the mechanisms that can account for the observation of the hydroxyl radical in aqueous solutions.

We were unable to detect the BMPO–OOH spin adduct resulting from direct $O_2^{\bullet-}$ trapping by BMPO under diode laser irradiation in PBS. Instead, we detected the spin adduct with the hydroxyl radical. There are two possible explanations of this observation: 1) all $O_2^{\bullet-}$ may act as a precursor of OH$^\bullet$; 2) the BMPO–OOH adduct may be formed, but cannot be observed due to its lifetime being too short. The presence of catalase inhibits the formation of the BMPO–OH radical adduct. Catalase splits hydrogen peroxide into water and molecular oxygen, and the observed inhibition of OH$^\bullet$ formation proves that hydroxyl radicals are not formed directly from the photosensitizer and molecular oxygen, but rather as a secondary thermal product. The addition of superoxide dismutase, a known scavenger of the superoxide ion, also inhibits the formation of the BMPO–OH radical adduct, corroborating the hypothesis that the hydroxyl radical is formed consecutively to other species such as the superoxide ion and hydrogen peroxide. The photogeneration of superoxide and its subsequent reactions to produce hydrogen peroxide can be described by the mechanism in Equations (15)–(19).

$$^3TDCPBSO_3H + {}^3O_2 \rightarrow TDCPBSO_3H^{+\bullet} + O_2^{\bullet-} \quad (15)$$

$$TDCPBSO_3H^{+\bullet} + O_2^{\bullet-} \rightarrow TDCPBSO_3^\bullet + HO_2^\bullet \quad (16)$$

$$2\,O_2^{\bullet-} + 2\,H^+ \rightarrow O_2 + H_2O_2 \quad (17)$$

$$HO_2^\bullet + HO_2^\bullet \rightarrow O_2 + H_2O_2 \quad (18)$$

$$HO_2^\bullet + O_2^{\bullet-} + H^+ \rightarrow O_2 + H_2O_2 \quad (19)$$

The rate of superoxide disproportionation [Eq. (17)] at pH 7.4 is reported as $2.4\times10^5\ M^{-1}s^{-1}$.[45] The disproportionation rate of the perhydroxyl radical [Eq. (18)] is $8.1\times10^5\ M^{-1}s^{-1}$.[46] The oxidation of superoxide by the perhydroxyl radical reflects the fact that $HO_2^\bullet$ is the more potent oxidant. The subsequent formation of the hydroxyl radical may proceed directly by Equations (20) and (21), but their rate constants, 16 and 3.7 M^{-1}s^{-1} in water,[46] are much slower

than the relatively rapid dismutation of the $HO_2^{\bullet}/O_2^{\bullet-}$ radicals.[47]

$$O_2^{\bullet-} + H_2O_2 \rightarrow O_2 + OH^{\bullet} + OH^- \quad (20)$$

$$HO_2^{\bullet} + H_2O_2 \rightarrow O_2 + OH^{\bullet} + H_2O \quad (21)$$

The Haber–Weiss reaction [Eq. (20)] was recently observed in the gas phase,[48] but remains controversial in water. Alternatively, we propose that bacteriochlorins may also lead to the hydroxyl radical through photocatalysis, [Eq. (22)], in view of the facile electron-transfer from $^3TDCPBSO_3H$ discussed above, although hydrogen peroxide is a worse electron acceptor than molecular oxygen.

$$^3TDCPBSO_3H + H_2O_2 \rightarrow TDCPBSO_3H^{+\bullet} + H_2O_2^{\bullet-} \rightarrow TDCPBSO_3^{\bullet} + OH^{\bullet} + H_2O \quad (22)$$

It has been suggested that the transient species $H_2O_2^-$ is accessed in a Franck–Condon transition in a dissociative electron attachment to H_2O_2 that produces $OH^{\bullet}$ and HO^-.[49] Given the very weakly exothermic electron transfer between $^3TDCPBSO_3H$ and O_2, we expect electron transfer to H_2O_2 to be endothermic and slow. Nevertheless, the relatively long lifetime of $^3TDCPBSO_3H$ in water gives us the opportunity to investigate the photoinduced electron transfer to H_2O_2.

Before addressing the excited-state reaction with H_2O_2, it is important to note that aqueous solutions of $TDCPBSO_3H$ are remarkably stable in the dark, even in the presence of H_2O_2. The half-life of this bacteriochlorin in aqueous solutions with $[H_2O_2]=5$ mM is approximately one week. We measured the lifetimes of $^3TDCPBSO_3H$ in N_2-saturated PBS solutions (pH 7.4) with various amounts of H_2O_2, at 20 °C. Figure 10 shows the reciprocals of the triplet lifetimes as a function of $[H_2O_2]$, from which we estimate the rate constant for electron transfer to H_2O_2, $k_{H_2O_2}=3\times10^7\,M^{-1}s^{-1}$. This is much higher than the rate constants of reactions shown in Equations (20) and (21), and makes photocatalysis the preferred mechanism for hydroxyl-radical generation by bacteriochlorins. This rate should correspond to an outer-sphere electron-transfer reaction that is endothermic by 5 kcal mol^{-1},[50] as expected from the low electron affinity of H_2O_2. It must be emphasized that in aerated solutions, electron transfer to H_2O_2 competes with quenching by O_2, which occurs with a rate constant of $^4/_9k_{diff}$. The production of the hydroxyl radical only becomes effective with the depletion of O_2 from the solution and the concomitant accumulation of H_2O_2.

Additional evidence for photocatalysis was found in the pH dependence of the photodegradation of $TDCPBSO_3H$. The bleaching is accelerated at lower pH and slowed at higher pH with respect to PBS solutions, under laser irradiation. Acidic media favour the formation of H_2O_2, but only in the presence of light does this species lead to efficient degradation of $TDCPBSO_3H$.

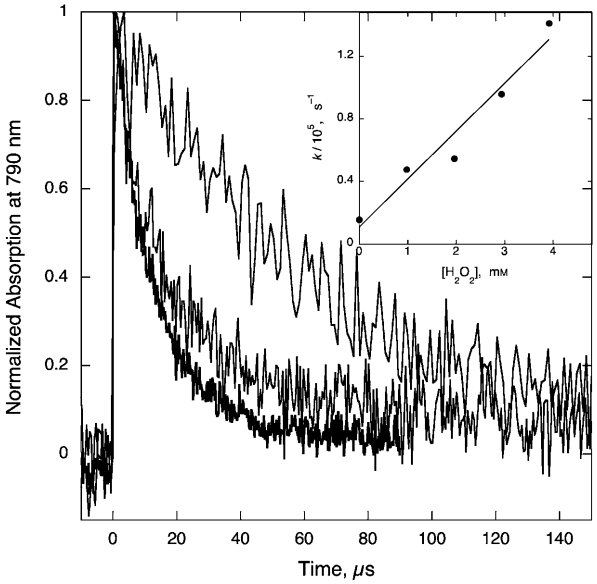

Figure 10. Decays of triplet $TDCPBSO_3H$ absorption at 790 nm in N_2-saturated PBS solutions with the following concentrations of H_2O_2: 0, 1 and 3 mM. The inset shows the H_2O_2 concentration dependence of the reciprocal of the triplet lifetimes.

The $OH^{\bullet}$ radical is a highly reactive oxidant and much more cytotoxic than singlet oxygen or the superoxide ion, and it may contribute significantly to the efficacy of PDT. However, hydroxyl-radical generation through photocatalysis is intrinsically limited by the amount of excited photosensitizer. On the other hand, it is very well known that $OH^{\bullet}$ is very efficiently produced in the Haber–Weiss/Fenton reaction, which consists of an iron reduction step by $O_2^{\bullet-}$ and an $OH^{\bullet}$ generation step through the Fenton reaction,[51] as given in Equations (23) and (24).

$$Fe^{3+} + O_2^{\bullet-} \rightarrow Fe^{2+} + O_2 \quad (23)$$

$$Fe^{2+} + H_2O_2 \rightarrow Fe^{3+} + OH^{\bullet} + OH^- \quad (24)$$

These reactions have been shown to take place in vivo.[52] Hence, on the basis of these reaction mechanisms, we argue that co-locating the ferrous ion with a bacteriochlorin photosensitizer may increase the efficacy of PDT.

The EPR spectra of $TDCPBSO_3H$ in the presence of DMPO in aerated DMSO under diode laser irradiation show that the superoxide ion is formed under these conditions. Since DMSO is an aprotic solvent, it prolongs the lifetime of $O_2^{\bullet-}$ and the stability of the DMPO–OOH adduct, favouring the observation of this adduct. In summary, these observations are consistent with the hypothesis that the superoxide radical is produced from halogenated bacteriochlorins, and that the superoxide radicals in turn form hydroxyl radicals in aqueous solutions.

The generation of $O_2^{\bullet-}$ in the simplified mechanism is competitive with the charge recombination in the charge-transfer complex [Eqs. (15) and (16) above]. This generation occurs by separation of the radical–ion pair, which is nearly

isoenergetic with the free ion in ethanol. A similar separation in acetonitrile takes place with a rate $k_{sep}=8\times10^8\ s^{-1}$.[53] It is reasonable to assume that the separation is slightly slower in ethanol, and we should have $k_{sep}\approx5\times10^8\ s^{-1}$. We defined before $k_3=k_{sep}+k_{-et}$ and determined the value of k_3. Now we can estimate $k_{-et}=2\times10^8\ s^{-1}$ for reactions with exothermicities $\Delta G^0_{-et}\approx-25$ kcal mol^{-1}. Charge recombination reactions are usually much faster at this ΔG^0_{-et}.[50,54] However, for radical–ion pairs formed from triplet states, charge recombination rates of this magnitude have been measured.[55] Thus, in polar solvents and for triplet donors with low oxidation potentials, it is possible to produce the superoxide ion.

Conclusion

The bacteriochlorins employed in this work can generate both singlet oxygen and superoxide ions. The quantum yields of singlet-oxygen generation are high, and the energy-transfer rates are accelerated by the presence of charge-transfer interactions. These bacteriochlorins are particularly interesting for photodynamic therapy (PDT) because of their strong absorption in the phototherapeutic window, photochemical stability, and wide range of 1-octanol/water solubilities. The detailed analysis of the mechanism of quenching of their triplet states by oxygen provides an important insight into this ubiquitous photochemical reaction. For the first time it has been possible to develop a quantitative understanding of the processes involved in the generation of singlet oxygen and superoxide ions, and to measure the elementary rates involved. Scheme 4 summarizes the information obtained on these systems. This scheme considers the possibility of singlet-oxygen generation from a CT complex. This can be regarded as a weakly exothermic charge recombination, $\Delta G^0_{-CT}\approx-4$ kcal mol^{-1}, which must compete with the very exothermic charge recombination to the ground state, $\Delta G^0_{-CT}\approx-25$ kcal mol^{-1}, and is likely to be inefficient for the $O_2/O_2^{\bullet-}$ pair unless favoured by spin conservation. This means that only the species in the singlet channel are likely to evolve along this channel.

The presence of a charge-transfer complex exacerbates the laser energy dependence of singlet-oxygen generation by triplet bacteriochlorins. Although bacteriochlorins generate singlet oxygen efficiently at low laser intensities, the amount of singlet oxygen that they generate at high laser intensities is much less than that of porphyrin sensitizers. Current protocols for PDT dosimetry are simply based on the product between the fluence rate of light (in units of W cm^{-2} or J cm^{-2} s^{-1}) and exposure time.[56] However, the full potential of bacteriochlorins can only be exploited if lower light intensities and longer irradiation times are employed in the therapy, which does not change the dosimetry, but changes the dosimetry mode. Repeating with bacteriochlorins the same protocols as with porphyrins is not efficient. It was recently reported that the laser fluence rate was a principal factor in PDT efficacy.[57] Empirically, it was found that compensating a decrease in laser power with an increase in photosensitizer dosage, which formally yields the same amount of singlet oxygen, leads to dramatically different PDT efficacies. The combination of lower laser power with higher photosensitizer dosage is the most effective.[57] This observation cannot be accommodated by the usual argument of molecular oxygen depletion at the irradiation site, but finds support in our mechanism of energy and electron transfer. Interestingly, molecular oxygen depletion and hydrogen peroxide accumulation in photosensitization by bacteriochlorins favours the photocatalytic pathway for the generation of the hydroxyl ion, which is one of the most potent reactive oxygen species. The generation of this ROS may be further enhanced by using ferrous iron as an adjuvant to PDT.

The mechanisms and kinetics of singlet-oxygen and superoxide-ion generation have been analyzed thoroughly. Intersystem crossing between triplet and singlet pathways occurs efficiently only in the charge-separated states. Singlet oxygen is formed preferentially from the encounter com-

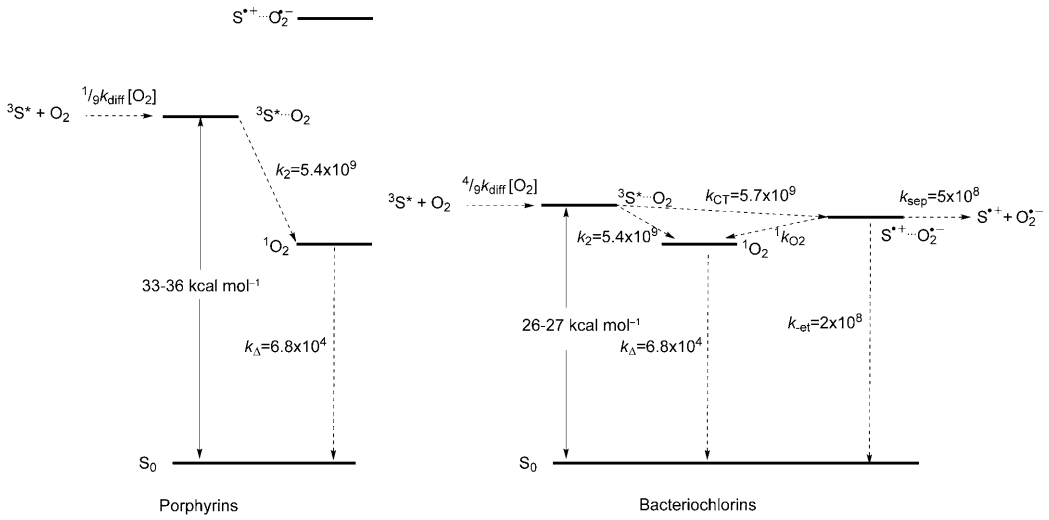

Scheme 4. Rates (in s^{-1}) and energies in the photosensitization of singlet oxygen and superoxide ion by porphyrins or bacteriochlorins.

plex, and the radical-ion pair is the precursor of the superoxide ion. The observed triplet decay constants are not a direct measure of the internal conversion in the encounter complex, to generate singlet oxygen, in the nCT channel. Nor are such decay constants a measure of the charge separation rates in the CT channel. In both cases it is necessary to refer to Equation (7) to obtain the actual internal conversion or charge separation rates. The correct interpretation of the observed rates may contribute to establishing more fundamental relations between the molecular structure of photosensitizers and the kinetics and thermodynamics of the reaction they initiate.

Experimental Section

Synthesis: The syntheses of 5,10,15,20-tetrakis(2,6-dichlorophenyl) porphyrin (TDCPP), followed the methods described in the literature.[21,58] In the chlorosulfonation of TDCPP, TDCPP (100 mg, 0.11×10^{-3} mol) and chlorosulfonic acid (6 mL) were stirred at 100 °C for 3 h. After cooling, chloroform (200 mL) was added, and the excess of chorosulfonic acid was washed out with water in a continuous process. The organic layer was dried, and after workup, the solvent was removed. The 5,10,15,20-tetrakis(2,6-dichloro-3-chlorosulfonylphenyl) porphyrin was obtained in rather pure form by this process, with a 90% yield, but, if necessary, the crude product can be further purified by silica gel column chromatography using chloroform as eluent. MS (FAB), *m/z*: 1285 $[M+H]^+$; ^{1}H NMR (300 MHz, $CDCl_3$): $\delta=8.66$–8.62 (m, 12H, β-*H* and Ph-*H*), 8.11–8.05 (m, 4H, Ph-*H*), −2.51 ppm (s, 2H, N*H*); elemental analysis calcd (%) for $C_{44}H_{18}N_4O_8Cl_{12}S_4$: C 41.15, H 1.41, N 4.36; found: C 40.70, H 1.60, N 4.30.

The desired porphyrin derivatives TDCPPSO$_3$H, TDCPPSNHethyl, and TDCPPSNHheptyl were obtained after reaction of 5,10,15,20-tetrakis(2,6-dichloro-3-chlorosulfonylphenyl) porphyrin with water, ethylamine, or heptylamine. The physical properties of the compounds are in good agreement with previously described data.[25]

The porphyrins TDCPPSO$_3$H, TDCPPSNHethyl, and TDCPPSNHheptyl were thoroughly mixed with *p*-toluenesulfonylhydrazide (1:35), placed in a degassed reactor, and heated to 150 °C for 10 min. This procedure yielded substantially pure bacteriochlorins TDCPBSO$_3$H, TDCPBSNHethyl, and TDCPBSNHheptyl. Purification and characterization details are presented elsewhere.[59]

Photochemistry: Absorption and luminescence spectra were recorded at room temperature with a Shimadzu UV-2100 spectrophotometer and SPEX Fluorolog 3.22 spectrophotometer, respectively. Most photochemical studies employed photosensitizer concentrations adjusted to produce absorbances in the 0.2–0.25 range at the excitation wavelengths. We found no evidence for sensitizer aggregation at these concentrations. The absorptions of both reference and sample solutions in fluorescence quantum yield measurements were matched at $\approx$0.2 at the excitation wavelength of 515.5 nm, and then the solutions were diluted by a factor of 10 before collecting the fluorescence. The fluorescence quantum yields were obtained from the ratio of the fluorescence bands of the samples vs. the reference, multiplied by the fluorescence quantum yield of the reference, after correction for the difference in refractive indexes between the sample and reference solutions. The reference employed was 5,10,15,20-tetrakis(2,6-dichlorophenyl) bacteriochlorin (TDCPB), for which $\Phi_F=0.012$ in toluene.[4]

Transient triplet–triplet absorption was obtained with an Applied Photophysics LKS.60 flash photolysis spectrometer with the R928 photomultiplier from Hamamatsu for detection and HP Infinium (500 MHz, 1 GSa s^{-1}) or Tektronix DPO 7254 (2.5 GHz, 40 GSa s^{-1}) oscilloscopes. An adaptation of this spectrometer allowed the detection of singlet-oxygen phosphorescence at room temperature. This emission was detected using a Hamamatsu R5509–42 photomultiplier, cooled to 193 K in a liquid nitrogen chamber (Products for Research, model PC176TSCE005). Excitation was achieved with the third harmonic of Nd:YAG lasers (Spectra-Physics Quanta Ray GCR 130, 5–6 ns FWHM, or EKSPLA PL 2143 A, 30 ps pulse width).

The modification of the spectrometer for time-resolved singlet-oxygen phosphorescence measurements involved the interposition of a Melles Griot cold mirror (03MCS005), which reflects more than 99% of the incident light in the 400–700 nm range, and of a Scotch RG665 filter. A 600 line diffraction grating was mounted in place of a standard one. This equipment allows spectral identification of the singlet-oxygen phosphorescence and measurement of the singlet-oxygen lifetime in the nanosecond and microsecond ranges. The filters employed are essential for eliminating from the infrared signal all harmonic contributions of the sensitizer emission in the 400–900 nm range. Singlet oxygen quantum yields in ethanol were obtained with a procedure described elsewhere,[36] using phenalenone as reference, for which $\Phi_\Delta=0.95\pm0.02$ in ethanol.[34]

Photoacoustic calorimetry (PAC) was performed with the front-face cell design.[60] The sample, reference and solvent solutions were flowed separately with a 1 mL min^{-1} rate (SSI chromatographic pump) through a cell of thickness 0.2 mm. They were irradiated at 355 nm with a Spectra-Physics Quanta Ray GCR 130 at a frequency of 10 Hz. A small fraction of the laser beam was reflected to a photodiode, used to trigger the transient recorder (Tektronix DSA 601, 1GSa/s). The photoacoustic waves, detected with a 2.25 MHz Panametrics transducer (model 5676) and captured by the transient recorder, were transferred to a PC for data analysis. In a typical PAC experiment, 200 waves of the sample, reference, and pure solvent were recorded and averaged in the same experimental conditions. Four sets of averaged sample, reference, and solvent waves were used for the data analysis at a given laser intensity, and four laser intensities were employed in each experiment. The different laser intensities are obtained by interposing neutral density filters with transmissions between 25 and 100%. The measurements were made using manganese 5,10,15,20-tetraphenylporphyrin (MnTPP) as photoacoustic reference (excitation at 355 nm).[21]

Electron paramagnetic resonance (EPR) measurements: Reactive oxygen species produced by irradiation of TDCPBSO$_3$H in phosphate buffer (PBS) or dimethylsulfoxide (DMSO) solutions, namely the hydroxyl radical and the superoxide ion, form adducts with various spin traps. Two spin traps were employed: 5,5-dimethylpyrroline-*N*-oxide (DMPO) and 5-tert-butoxycarbonyl 5-methyl-1-pyrroline N-oxide (BMPO). The adducts formed were identified by EPR. EPR measurements were performed at room temperature using a Bruker ESP 300 spectrometer (IBM Instruments Inc.). The EPR spectra were recorded under in situ irradiation with a Hamamatsu diode laser (748 nm). Typical instrument settings for superoxide detection were: microwave power 10 mW, modulation amplitude 0.8 G, sweep width 60.0 G. Slightly different settings were employed to register the BMPO−OH adduct: microwave power 4 mW, modulation amplitude 0.2 G, narrow scan range 60 G, and 20 scans were recorded for each spectrum. The Hamamatsu diode laser, type LA0873, S/N M070301, delivered 100 mW at 748 nm. This diode laser was controlled by a ThorLabs 500 mA ACC/APC Laser Diode Controller. The laser energies of this and the other higher-energy lasers employed in this work were regularly checked with an Ophir model AN/2E laser power meter. The EPR spectra were simulated using the software EPRsim32.[61] The PBS employed in these measurements was previously treated with chelating resin, Chelex 100, in order to remove any contaminating metal ions that may catalyze the decomposition of peroxides. DMPO was first purified with activated charcoal/benzene, and then a 1.0 M stock concentration was determined spectrophotometrically using $\varepsilon_{226}=7200\,M^{-1}cm^{-1}$.

The EPR experiments were performed in the presence of 30–80 μM of TDCPBSO$_3$H and 40 mM BMPO in PBS, or with 50 μM of TDCPBSO$_3$H and 100 mM DMPO in DMSO, under the following conditions: air-saturated solutions in the dark, nitrogen-saturated solutions irradiated for 1–15 min with the diode laser, air-saturated solutions irradiated for 1–15 min with the diode laser in the presence of catalase (30 μg mL^{-1}) or superoxide dismutase (50 μg mL^{-1}).

Acknowledgements

This work was funded by Fundação para a Ciência e a Tecnologia (Portugal) and FEDER (project no. ERA-CHEM/0002/2008). Support from CCDRC and Câmara Municipal de Coimbra is gratefully acknowledged. C.J.P.M. and E.F.F.S. thank FCT for grants BD/37652/2007 and BD/46658/2008. This work was also supported in part by the National Centre for Research and Development (Era Chemistry grant nr. 60 303). The authors thank Dr. M. Elas for providing us with the spin probe (mHCTPO) and spin trap (BMPO), Prof. Z. Sojka for the EPRsim32 simulation program, and Dr. K. Kruczała for his help with EPR spectra simulation.

[1] P.-C. Lo, J.-D. Huang, D. Y. Y. Cheng, E. Y. M. Chan, W.-P. Fong, W.-H. Ko, D. K. P. Ng, *Chem. Eur. J.* **2004**, *10*, 4831–4838.
[2] J. Arnbjerg, A. Jiménez-Banzo, M. J. Paterson, S. Nonell, J. I. Borrel, O. Christiansen, P. R. Ogilby, *J. Am. Chem. Soc.* **2007**, *129*, 5188–5199.
[3] C. Liu, M. P. Dobhal, M. Ethirajan, J. R. Missert, R. K. Pandey, S. Balasubramanian, D. K. Sukumaran, M. Zhang, K. M. Kadish, K. Ohkubo, S. Fukuzumi, *J. Am. Chem. Soc.* **2008**, *130*, 14311–14323.
[4] M. Pineiro, A. M. d. A. Rocha Gonsalves, M. M. Pereira, S. J. Formosinho, L. G. Arnaut, *J. Phys. Chem. A* **2002**, *106*, 3787–3795.
[5] M. M. Pereira, C. J. P. Monteiro, A. V. C. Simões, S. M. A. Pinto, L. G. Arnaut, G. F. F. Sá, E. F. F. Silva, L. B. Rocha, S. Simões, S. J. Formosinho, *J. Porphyrins Phthalocyanines* **2009**, *13*, 567–573.
[6] C. Hopper, *Lancet Oncol.* **2000**, *1*, 212–219.
[7] T. J. Dougherty, *J. Clin. Laser Med. Sci.* **2002**, *20*, 3–7.
[8] C. M. Moore, D. Pendse, M. Emberton, *Nat. Clin. Pract. Urol.* **2009**, *6*, 18–30.
[9] F. H. van Duijnhoven, J. P. Rovers, K. Engelmann, Z. Krajina, S. F. Purkiss, F. A. N. Zoetmulder, T. J. Vogl, O. T. Terpstra, *Ann. Surg. Oncol.* **2005**, *12*, 808–816.
[10] J. Trachtenberg, A. Bogaards, R. A. Weersink, M. A. Haider, A. Evans, S. A. McCluskey, A. Scherz, M. R. Gertner, C. Yue, S. Appu, A. Aprikian, J. Savard, B. C. Wilson, M. Elhilali, *J. Urol.* **2007**, *178*, 1974–1979.
[11] M. Hoebeke, H. J. Schuitmaker, L. E. Jannink, T. M. A. R. Dubbelman, A. Jakobs, A. Van de Vorst, *Photochem. Photobiol.* **1997**, *66*, 502–508.
[12] Y. Vakrat-Haglili, L. Weiner, V. Brumfeld, A. Brandis, Y. Salomon, B. McIlroy, B. C. Wilson, A. Pawlak, M. Rozanowska, T. Sarna, A. Scherz, *J. Am. Chem. Soc.* **2005**, *127*, 6487–6497.
[13] S. Fukuzumi, K. Ohkubo, X. Zheng, Y. Chen, R. K. Pandey, R. Zhan, K. M. Kadish, *J. Phys. Chem. B* **2008**, *112*, 2738–2746.
[14] L. W. Oberley, G. R. Buettner, *Cancer Res.* **1979**, *39*, 1141–1149.
[15] C. Schweitzer, R. Schmidt, *Chem. Rev.* **2003**, *103*, 1685–1757.
[16] F. Wilkinson, A. A. Abdel-Shafi, *J. Phys. Chem. A* **1997**, *101*, 5509–5516.
[17] A. A. Abdel-Shafi, F. Wilkinson, *J. Phys. Chem. A* **2000**, *104*, 5747–5757.
[18] A. A. Abdel-Shafi, F. Wilkinson, *Phys. Chem. Chem. Phys.* **2002**, *4*, 248–254.
[19] R. Schmidt, F. Shafii, C. Schweitzer, A. A. Abdel-Shafi, F. Wilkinson, *J. Phys. Chem. A* **2001**, *105*, 1811–1817.
[20] R. Schmidt, *Photochem. Photobiol.* **2006**, *82*, 1161–1177.
[21] M. Pineiro, A. L. Carvalho, M. M. Pereira, A. M. d. A. R. Gonsalves, L. G. Arnaut, S. J. Formosinho, *Chem. Eur. J.* **1998**, *4*, 2299–2307.
[22] B. Wang, P. R. Ogilby, *J. Photochem. Photobiol. A* **1995**, *90*, 85–89.
[23] L. G. Arnaut, S. J. Formosinho, A. M. da Silva, *J. Photochem.* **1984**, *27*, 185–203.
[24] E. G. Azenha, A. C. Serra, M. Pineiro, M. M. Pereira, J. Seixas de Melo, L. G. Arnaut, S. J. Formosinho, A. M. d. A. R. Gonsalves, *Chem. Phys.* **2002**, *280*, 177–190.
[25] C. J. P. Monteiro, M. M. Pereira, S. M. A. Pinto, A. V. C. Simões, G. F. F. Sá, L. G. Arnaut, S. J. Formosinho, S. Simões, M. F. Wyatt, *Tetrahedron* **2008**, *64*, 5132–5138.
[26] M. Pineiro, PhD Thesis, University of Coimbra (Portugal), **2001**.
[27] A. S. M. Ressurreição, M. Pineiro, L. G. Arnaut, A. M. d. A. R. Gonsalves, *J. Porphyrins Phthalocyanines* **2007**, *11*, 50–57.
[28] D. J. Quimby, F. R. Longo, *J. Am. Chem. Soc.* **1975**, *97*, 5111–5117.
[29] S. K. Pandey, A. L. Gryshuk, A. Graham, K. Ohkubo, S. Fukuzumi, M. P. Dodhal, G. Zheng, Z. Ou, R. Zhan, K. M. Kadish, A. Oseroff, S. Ramaprasad, R. K. Pandey, *Tetrahedron* **2003**, *59*, 10059–10073.
[30] M. Pineiro, M. M. Pereira, A. M. d. A. R. Gonsalves, L. G. Arnaut, S. J. Formosinho, *J. Photochem. Photobiol. A* **2001**, *138*, 147–157.
[31] A. Harriman, *J. Chem. Soc. Faraday Trans. 2* **1981**, *77*, 1281–1291.
[32] S. L. Murov, I. Carmichael, G. L. Hug, *Handbook of Photochemistry*, Marcel Dekker, New York, **1993**.
[33] M. A. J. Rodgers, *J. Am. Chem. Soc.* **1983**, *105*, 6201–6205.
[34] R. Schmidt, C. Tanielian, R. Dunsbach, C. Wolff, *J. Photochem. Photobiol. A* **1994**, *79*, 11–17.
[35] R. Schmidt, C. Tanielian, *J. Phys. Chem. A* **2000**, *104*, 3177–3180.
[36] J. M. Dabrowski, M. M. Pereira, L. G. Arnaut, C. J. P. Monteiro, A. F. Peixoto, A. Karocki, K. Urbanska, G. Stochel, *Photochem. Photobiol.* **2007**, *83*, 897–903.
[37] C. Tanielian, C. Wolff, *J. Phys. Chem. A* **1995**, *99*, 9825–9830.
[38] H. Zhao, J. Joseph, H. Zhang, H. Karoui, B. Kalyanaraman, *Free Radical Biol. Med.* **2001**, *31*, 599–606.
[39] A. Weller, *Z. Phys. Chem.* **1982**, *133*, 93–98.
[40] C. Huang, M. Tian, Y. Yang, F. Guo, M. Wang, *J. Electroanal. Chem.* **1989**, *272*, 179–184.
[41] J. Fajer, D. C. Borg, A. Forman, R. H. Felton, D. Dolphin, L. Vegh, *Proc. Natl. Acad. Sci. USA* **1974**, *71*, 994–998.
[42] M. Tezuka, Y. Ohkatsu, T. Osa, *Bull. Chem. Soc. Jpn.* **1976**, *49*, 1435–1436.
[43] K. Kawaoka, A. U. Khan, D. R. Kearns, *J. Chem. Phys.* **1967**, *46*, 1842–1853.
[44] M. Bodesheim, M. Schütz, R. Schmidt, *Chem. Phys. Lett.* **1994**, *221*, 7–14.
[45] C. Rizzi, A. Samouilov, V. K. Kutala, N. L. Parinandi, J. L. Zweier, P. Kuppusamy, *Free Radical Biol. Med.* **2003**, *35*, 1608–1618.
[46] B. G. Ershov, A. V. Gordeev, *Radiat. Phys. Chem.* **2008**, *77*, 928–935.
[47] J. Weinstein, B. H. J. Bielski, *J. Am. Chem. Soc.* **1979**, *101*, 58–62.
[48] S. J. Blanksby, V. M. Bierbaum, G. B. Allison, S. Kato, *Angew. Chem.* **2007**, *119*, 5036–5038.
[49] D. Nandi, E. Krishnakumar, A. Rosa, W.-F. Schmidt, E. Illenberger, *Chem. Phys. Lett.* **2003**, *373*, 454–459.
[50] S. J. Formosinho, L. G. Arnaut, R. Fausto, *Prog. React. Kinet.* **1997**, *23*, 1–90.
[51] T. Nunoshiba, F. Obata, A. C. Boss, S. Oikawa, T. Mori, S. Kawanishi, K. Yamamoto, *J. Biol. Chem.* **1999**, *274*, 34832–34837.
[52] J. A. Imlay, S. M. Chin, S. Linn, *Science* **1988**, *240*, 640–642.
[53] I. R. Gould, S. Farid, *J. Phys. Chem.* **1992**, *96*, 7635–7640.
[54] C. Serpa, P. J. S. Gomes, L. G. Arnaut, S. J. Formosinho, J. Pina, J. Seixas de Melo, *Chem. Eur. J.* **2006**, *12*, 5014–5023.
[55] C. Serpa, L. G. Arnaut, *J. Phys. Chem. A* **2000**, *104*, 11075–11086.
[56] *General Medical Physics Committee Task Group #5, Photodynamic Therapy Dosimetry*, Vol. 88 (Ed.: AAPM), AAPM, College Park, **2005**.
[57] M. Seshadri, D. A. Bellnier, L. A. Vaughan, J. A. Spernyak, R. Mazurchik, T. H. Foster, B. W. Henderson, *Clin. Cancer Res.* **2008**, *14*, 2796–2805.
[58] A. M. d. A. R. Gonsalves, J. M. T. B. Varejão, M. M. Pereira, *J. Heterocycl. Chem.* **1991**, *28*, 635–640.
[59] M. M. Pereira, C. J. P. Monteiro, A. V. C. Simões, S. M. A. Pinto, G. F. F. Sa, E. F. F. Silva, L. Rocha, J. M. Dąbrowski, S. J. Formosinho, S. Simões, L. G. Arnaut, unpublished results.
[60] L. G. Arnaut, R. A. Caldwell, J. E. Elbert, L. A. Melton, *Rev. Sci. Instrum.* **1992**, *63*, 5381–5389.
[61] T. Spalek, P. Pietrzyk, Z. Sojka, *J. Chem. Inf. Model.* **2005**, *45*, 18–29.

Received: January 15, 2010
Please note: Minor changes have been made to this manuscript since its publication in *Chemistry—A European Journal* Early View. The Editor.
Published online: June 22, 2010

